

# Solution-Processed Ultrahigh PHPS Gas Barriers with Glass-like Performance

Tatsuki Sasaki<sup>1</sup>, Lina Sun<sup>2</sup>, Yu Kurosawa<sup>2</sup>, Tatsuhiro Takahashi<sup>1</sup>, Yoshiyuki Suzuri<sup>2</sup>

suzuri@yz.yamagata-u.ac.jp

<sup>1</sup> Department of Organic Materials Science, Yamagata Univ., Jonan 4-3-16, Yonezawa, Yamagata 992-8510, Japan

<sup>2</sup> Innovation Center for Organic Electronics (INOEL), Yamagata Univ., Arcadia 1-808-48, Yonezawa, Yamagata 992-0119, Japan

Keywords: water vapor barrier films, solution processes, perhydropolysilazanes, vacuum UV, organic light-emitting diodes

## ABSTRACT

We report all-solution-processed gas barriers using perhydropolysilazane (PHPS)-derived SiN films densified by vacuum ultraviolet (VUV) irradiation in a nitrogen atmosphere. The appropriate PDSN thickness and irradiated VUV dose afford an excellent WVTR of  $4.8 \times 10^{-5} \text{ g m}^{-2} \text{ day}^{-1}$ , which makes it one of the best-performing water vapor barriers recorded to date.

## 1 Introduction

Gas barrier films are essential components of display applications because they can effectively protect various products. Flexible organic light-emitting diodes (FOLEDs) are particularly sensitive to water vapor compared to other electronic products. Therefore, water vapor barriers are essential for the realization of FOLED displays that are expected to become widespread. The water vapor transmission rate (WVTR) is used as an indicator of the barrier performance. Requirements for gas barriers with WVTR less than  $10^{-5} \text{ g m}^{-2} \text{ day}^{-1}$  for FOLEDs are currently being discussed.<sup>1</sup> According to some reports, a barrier performance on the order of  $10^{-5} \text{ g m}^{-2} \text{ day}^{-1}$  can result in long lifetimes comparable to those with glass lids<sup>2,3</sup>.

Ultrahigh barrier performance with WVTR less than  $10^{-5} \text{ g m}^{-2} \text{ day}^{-1}$  has been achieved using dense inorganic layers fabricated by vacuum processes, for example, chemical vapor deposition and atomic layer deposition. However, the resource efficiency of the vacuum process is low, which means that the process generates a large amount of waste. The low deposition rate of the vacuum process is also a significant problem. In addition, considering the complicated process cycles in vacuum and under atmospheric pressure, the productivity can be even worse. By contrast, solution-processed gas barriers can simultaneously realize high resource efficiency, high throughput, and low fabrication cost. Furthermore, they can be applied both by wet coatings and by printing. Therefore, solution-processed gas barriers are considered a promising technology, which may play a significant role in manufacturing in the future.

Perhydropolysilazane (PHPS) containing an Si–N main chain has recently attracted much attention as a soluble precursor for dense inorganic layers. Vacuum ultraviolet (VUV,  $10 \text{ nm} < \lambda < 200 \text{ nm}$ ) irradiation in a

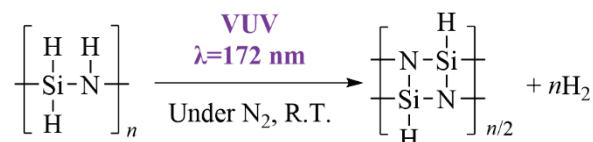


**Fig. 1** Vacuum ultraviolet (VUV) photochemical conversion of perhydropolysilazane (PHPS) into the SiN layers in a nitrogen atmosphere.

nitrogen atmosphere at room temperature can convert PHPS layers into amorphous SiN layers (Fig.1). In 2019, we reported all-solution-processed gas barriers made using PHPS-derived SiN (PDSN), with WVTR reaching the order of  $10^{-3} \text{ g m}^{-2} \text{ day}^{-1}$ , which is one of the best gas barrier performances of solution-processed gas barriers to date.<sup>4</sup> The room-temperature process, thin thickness (total thickness  $< 1 \mu\text{m}$ ), and optical transparency in the UV-vis region are also advantages of the gas barriers. In 2021, we analyzed the VUV-induced densification process to develop guidelines for improving the barrier performance of PDSN layers.<sup>5</sup> We found that dense PDSN layers with refractive index distribution in the direction of thickness were formed by VUV-induced Si–N network formation and atomic rearrangement that can decrease the free volume in the PDSN layers. Based on these results, we can expect that the thickness and amount of irradiated VUV light (VUV dose) are key parameters in determining the barrier performance. However, the relationship between these parameters, densification, and the resulting barrier performance has not been investigated.

In this study, we investigated the relationship between the barrier structures using PDSN layers and WVTR to achieve two-orders WVTR improvement of the solution-processed gas barriers from the best performance to date of  $10^{-3} \text{ g m}^{-2} \text{ day}^{-1}$  to  $10^{-5} \text{ g m}^{-2} \text{ day}^{-1}$ , which is close to the performance of vacuum-processed inorganic layers and glass. Considering the findings of the effect of VUV dose on the densification and the refractive index distribution with the high density near the surfaces, we especially focused on understanding the relationship between VUV dose–densification–WVTR and PDSN thickness–WVTR.

## 2 Experiment

### 2.1 Gas barrier preparation

All of the processes, including the precursor solution preparation, spin-coating, and UV and VUV irradiation were performed in an N<sub>2</sub>-filled glovebox. The PHPS solutions with different concentrations were prepared by diluting a 20 wt.% PHPS solution (in DBE solvent, without catalysts, Shin-Etsu Chemical) with anhydrous DBE (99.3%, Sigma-Aldrich) to obtain different layer thicknesses. The solutions were spin-coated on PI film /stress relaxation layer substrates or Si (100) substrates at 6000 rpm for 30 s. The layers were then exposed to VUV light with  $\lambda=172$  nm (FLAT EXCIMER, intensity to sample surfaces: 20 mW cm<sup>-2</sup>, Hamamatsu Photonics) at a stage temperature of <50 °C. The doses were controlled by varying the irradiation time.

### 2.2 Gas barrier characterization

The WVTR of the prepared gas barriers was measured by the modified differential pressure method with an attached support (MA method) on a Super-Detect (effective permeation area: 40 mm $\Phi$ , MORESCO) at 40 °C and 90% relative humidity. The MA method has a high sensitivity of 10<sup>-6</sup> g m<sup>-2</sup> day<sup>-1</sup> or less, with a shorter time than conventional methods.<sup>6</sup> To obtain the refractive index ( $n$  at 850 nm) and layer thickness, variable angle spectroscopic ellipsometry (VASE) measurements were conducted using a VASE 32 spectroscopic ellipsometer (J.A.Woollam). The angles of incident light ranged from 45° to 75° in steps of 5°. The experimental ellipsometric parameters ( $\Psi$  and  $\Delta$ ) of the PDSN layers were analyzed using a four-layer optical model containing SiO<sub>2</sub> and three single-layer models with Gaussian oscillators, as previously described.<sup>5</sup>

## 3 Results and Discussion

### 3.1 WVTR evaluation

For the structure with PDSN layers spin-coated on the PI/stress relaxation layer substrates, Fig. 2 shows the dependence of WVTR on both VUV dose irradiated to PHPS layers and the PDSN layer thickness. The WVTR

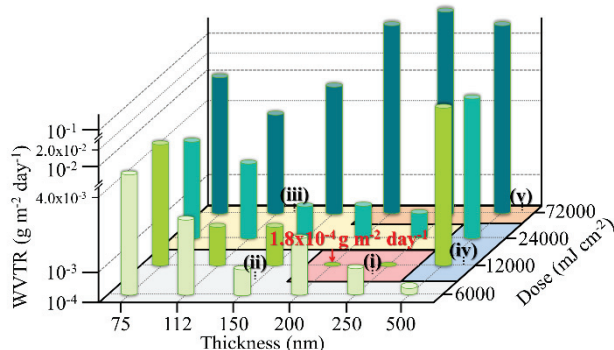


**Fig. 2** WVTR versus PDSN layer thickness (at the VUV dose of 6000 mJ cm<sup>-2</sup>) and VUV dose, including region references (i)–(v).

values of the PI film and the PI/stress relaxation layer structure were 9.0 g m<sup>-2</sup> day<sup>-1</sup> and 1.0 g m<sup>-2</sup> day<sup>-1</sup>, respectively. The barrier performance is much poorer than that of the PDSN layers. Therefore, the PI films and stress relaxation layers do not contribute to the barrier performance. As shown in Fig. 2, WVTR showed an optimum point for both VUV dose and PHPS layer thickness. In particular, in region (i) of Fig. 2, the PDSN layers with 200 nm and 250 nm (VUV dose: 12000 mJ cm<sup>-2</sup>) show almost the same WVTR of  $\sim 1.0 \times 10^{-4}$  g m<sup>-2</sup> day<sup>-1</sup>, which is an excellent barrier value. The WVTRs at 200 nm and 12000 mJ cm<sup>-2</sup> are in the range of 1.2–2.6 $\times 10^{-4}$  g m<sup>-2</sup> day<sup>-1</sup> (Sample: 3 samples, average value: 1.8 $\times 10^{-4}$  g m<sup>-2</sup> day<sup>-1</sup>, standard deviation: 7.2 $\times 10^{-5}$  g m<sup>-2</sup> day<sup>-1</sup>).

### 3.2 Effect of VUV Dose and Thickness on WVTR

To interpret the trend of the WVTR values from the viewpoint of the densification process, Fig. 3a shows the fitting results in the ellipsometry measurement for the PHPS and PDSN layers with different VUV doses. As the refractive indices of silicon nitride layers are generally proportional to their layer densities, the densification can be evaluated from the refractive index. The PHPS and PDSN layers were fitted using a single-layer model and a four-layer model. Although the small penetration depth of VUV light owing to the high absorption coefficient in the VUV region of the PHPS layers causes a continuous refractive index distribution in the direction of the layer thickness, the experimental ellipsometric parameters ( $\Psi$  and  $\Delta$ ) of the PDSN layers were fitted well by the four-layer model (MSE: <8.0).

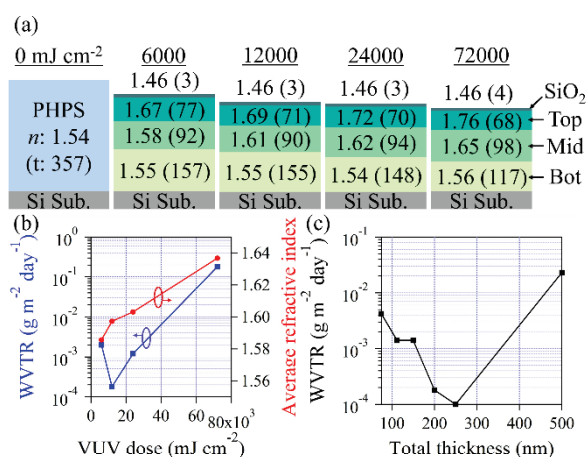


**Fig. 3** Relationship between the ellipsometry results (refractive index ( $n$ ) and layer thickness ( $t$ )) and WVTR values of PDSN layers. (a) Optical models for the PHPS and PDSN layers with different VUV doses on Si substrates in the ellipsometry measurements. (b) Comparison of WVTR values and average refractive index with VUV dose at a layer thickness of 200 nm. (c) Relationship between WVTR values and PDSN layer thickness at a VUV dose of 12000 mJ cm<sup>-2</sup>.

The refractive indices of the Top and Mid layers increased as a result of the VUV irradiation, whereas that of the Bot layers almost did not change. The refractive index increase is caused by two densification process: Si–N network formation and atomic rearrangement. VUV irradiation in a nitrogen atmosphere triggers the photochemical reaction, forming the Si–N network (Fig. 1). Because VUV light can also cleave Si–N bonds, the atomic rearrangement of the Si–N network can be caused by repeated bond cleavage and reformation cycles, and reduces the free volume<sup>5</sup>.

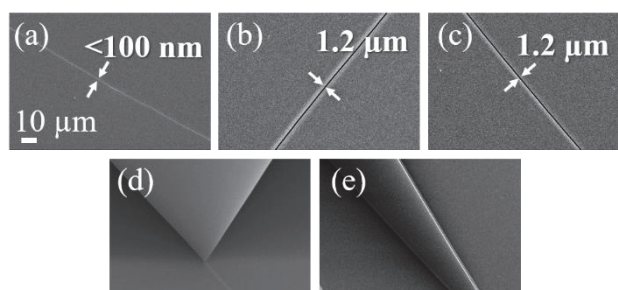
The average refractive index versus VUV dose at a layer thickness of 200 nm is compared with WVTR values in Fig. 3b. The average refractive index was calculated from the refractive index distribution obtained from ellipsometry. The average refractive index increases with VUV dose, and the densification of the PDSN layers is expected to improve the barrier performance. Contrary to expectation, the WVTR at 12000 mJ cm<sup>-2</sup> is a minimum value, and the barrier performance is deteriorated by further irradiation of more than 24000 mJ cm<sup>-2</sup>. This means that barrier performance is not determined by density alone.

Fig. 3c shows the layer thickness dependence of the WVTR values at a VUV dose of 12000 mJ cm<sup>-2</sup>. The WVTR value decreases as the layer becomes thicker, up to 250 nm, but the 500 nm layers show a significantly high WVTR value. Densified Top and Mid layers (Fig. 3a) can act as effective water vapor barrier layers. The sum of the Top and Mid layer thicknesses is approximately 170 nm, regardless of the VUV dose in the range of 6000–72000 mJ cm<sup>-2</sup>. When the total thickness is less than 170 nm, the barrier performance can degrade because of the lack of an effective barrier layer. In Fig. 3c, the barrier performance is low by one order of magnitude when the thickness is less than 150 nm, and the barrier performance degrades as the total thickness decreases; thus, Top and Mid layers can be the effective barrier layers. On the other hand, when the total thickness is sufficiently higher than 170 nm, it is expected that there will be no change in the effective barrier thickness. However, at a thickness of 500 nm, performance degradation of more than two orders of magnitude was observed. These results show that excessive VUV irradiation and a thick layer degrade the barrier performance. Again, these dependencies of VUV dose and thickness cannot be explained solely by densification. Barrier performance can be affected by barrier defects (cracks, pinholes, etc.); they can be formed according to the VUV dose and thickness, as well as density.

### 3.3 Defect Observation

Scanning electron microscopy (SEM) images of representative samples from each region of Fig. 2 after the WVTR measurements were obtained to check whether defects were formed, and their sizes were measured (Fig.

4). No defects were found in the samples from regions (i) and (ii) (Fig. 4a). Whereas excellent WVTR values of  $\sim 1.0 \times 10^{-4}$  g m<sup>-2</sup> day<sup>-1</sup> were achieved in region (i), the samples in region (ii) presented worse WVTRs on the order of  $10^{-3}$  g m<sup>-2</sup> day<sup>-1</sup> despite having no defects. This is probably due to the insufficient densification by the small VUV dose and the small total thickness being less than the effective barrier thickness (170 nm). In contrast, cracks were clearly observed in the samples from regions (iv) and (v) (Fig. 4 b-e). The cracks observed in the samples (thickness: 500 nm, VUV dose: 12000 or 24000 mJ cm<sup>-2</sup>) from region (iv) could be caused by the high thickness (Fig. 4 b and c). In the samples of region (v) with very high thickness and large VUV dose, we observed both cracks and delamination, leading to extremely low barrier performance (WVTR:  $\sim 10^{-1}$  g m<sup>-2</sup> day<sup>-1</sup>) (Fig. 4d and e). In region (iii), although we observed cracks only in a sample (thickness: 150 nm, VUV dose: 72000 mJ cm<sup>-2</sup>) as shown in Fig. 4a, nano cracks (which cannot be observed on SEM measurement) could be formed in the samples under other conditions in region (iii). The nano cracks could lead to the lower barrier performance (WVTR:  $\sim 10^{-3}$  g m<sup>-2</sup> day<sup>-1</sup>) than that in region (i) (WVTR:  $\sim 10^{-4}$  g m<sup>-2</sup> day<sup>-1</sup>). The crack width of the sample in region (iii) (WVTR:  $\sim 10^{-3}$  g m<sup>-2</sup> day<sup>-1</sup>) was only <100 nm, and that in region (iv) (WVTR:  $\sim 10^{-2}$  g m<sup>-2</sup> day<sup>-1</sup>) was approximately 1.2  $\mu$ m, indicating that the barrier performance deteriorated as the crack width increased. Cracks expanded with increasing VUV irradiation dose



**Fig. 4** Scanning electron microscopy (SEM) images of the PI/PDMS/PDSN barrier samples prepared under different conditions, taken after WVTR measurements had been obtained. Because there is a variation in the crack width, as regarding the samples from regions (iii)–(iv), we selected the cracks that were most frequently observed as the representative SEM images. (a) Region: (iii), Thickness: 150 nm, Dose: 72000 mJ cm<sup>-2</sup>, WVTR:  $10^{-3}$  g m<sup>-2</sup> day<sup>-1</sup> (b) Region: (iv), Thickness: 500 nm, Dose: 12000 mJ cm<sup>-2</sup>, WVTR:  $10^{-2}$  g m<sup>-2</sup> day<sup>-1</sup> (c) Region: (iv), Thickness: 500 nm, Dose: 24000 mJ cm<sup>-2</sup>, WVTR:  $10^{-2}$  g m<sup>-2</sup> day<sup>-1</sup> (d) Region: (v), Thickness: 250 nm, Dose: 72000 mJ cm<sup>-2</sup>, WVTR:  $10^{-1}$  g m<sup>-2</sup> day<sup>-1</sup> (e) Region: (v), Thickness: 500 nm, Dose: 72000 mJ cm<sup>-2</sup>, WVTR:  $10^{-1}$  g m<sup>-2</sup> day<sup>-1</sup>.

and thickness, suggesting increased internal stress in the PDSN layers.

### 3.4 Solution-processed ultrahigh gas barrier

Fig. 5 shows the comparison of WVTR value of the one unit and three units structures. One unit is composed of two layers (stress relaxation layer/PDSN) on a PI film and three units are alternating stacks (stress relaxation layer/PDSN x 3 units = 6 layers). The WVTR of three units was reduced to  $4.8 \times 10^{-5} \text{ g m}^{-2} \text{ day}^{-1}$  from  $2.2 \times 10^{-4} \text{ g m}^{-2} \text{ day}^{-1}$  (one unit). The barrier performance of the three units is two orders of magnitude higher than the best performance to date. Notably, the total thickness of the three units structure is only 990 nm. Thinner barrier structures are advantageous for flexibility.

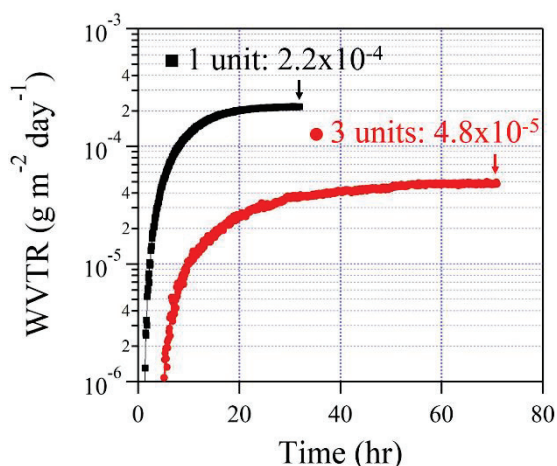


**Fig. 5** The WVTR of the 1 unit and 3 units gas barriers (PI/stress relaxation layer/PDSN (thickness: 200 nm, VUV dose:  $12000 \text{ mJ cm}^{-2}$ )).

## 4 Conclusions

In this study, we investigated the relationship between VUV dose–densification–WVTR and thickness–WVTR for solution-processed gas barriers using SiN layers derived from PHPS layers by VUV irradiation in a nitrogen atmosphere at room temperature. We found that the barrier performance significantly depends on the layer thickness and VUV dose, and only one PHPS layer (1 unit) achieved excellent WVTR ( $1.4 \times 10^{-4} \text{ g m}^{-2} \text{ day}^{-1}$  at  $40 \text{ }^\circ\text{C}$  and 90% relative humidity) under specific conditions (thickness of 200 nm, VUV dose of  $12000 \text{ mJ cm}^{-2}$ ). We also found that there is an optimal point in the WVTR values obtained by varying the layer thickness and VUV dose, owing to VUV irradiation-induced densification and crack formation attributed to the densification during the VUV reaction. Furthermore 3 units structure achieved extremely low WVTR values ( $4.8 \times 10^{-5} \text{ g m}^{-2} \text{ day}^{-1}$ ). The barrier performance on the order of  $10^{-5} \text{ g m}^{-2} \text{ day}^{-1}$  is close to the performance of glass and the best results ever recorded for a solution-processed gas barrier. This value represents a two-orders improvement in barrier performance over the best

reported performance. Notably, we achieved WVTR values with very small total layer thicknesses of 330 nm and 990 nm (1 unit and 3 units, respectively). Therefore, the gas barrier using VUV-irradiated PHPS layers is a promising candidate for components of flexible display.

## ACKNOWLEDGMENT

This work was financially supported by JSPS KAKENHI (Grant Number: 20K05640), the JST-COI Program (Grant Number: JPMJCE1312), and JST-OPERA. program (Grant Number: JPMJOP1844, Japan) and JST A-STEP program (Grant Number: JPMJTR21T8). The authors thank M. S. M. Kimura and M. S. T. Kaneko (Shin-Etsu Chemical Co., Ltd.) for supplying perhydropolysilazane, and Xenomax – Japan Co. Ltd. for supplying Xenomax.

## References

- [1] A. Uddin, M. B. Upama, H. Yi, and L. Duan, “Encapsulation of Organic and Perovskite Solar Cells: A Review” *Coatings*, Vol. 9, No. 65 (2019)
- [2] J. Meyer, D. Schneidenbach, T. Winkler, S. Hamwi, T. Weimann, P. Hinze, S. Ammermann, H.-H. Johannes, T. Riedl, and W. Kowalsky, “Reliable thin film encapsulation for organic light emitting diodes grown by low-temperature atomic layer deposition” *Appl. Phys. Lett.*, vol. 94, No. 23305 (2009).
- [3] Y. C. Han, C. Jang, K. J. Kim, K. C. Choi, K.H. Jung, B.-S. Bae, “The encapsulation of an organic light-emitting diode using organic–inorganic hybrid materials and MgO” *Org. Electron*, Vol. 12, No. 4, pp. 609-613 (2011).
- [4] L. Sun, K. Uemura, T. Takahashi, T. Yoshida, and Y. Suzuri, “Interfacial Engineering in Solution Processing of Silicon-Base Hybrid Multilayer for High Performance Thin Film Encapsulation” Vol. 11, No. 46, pp. 43425-43432 (2019).
- [5] T. Sasaki, L. Sun, Y. Kurosawa, T. Takahashi, and Y. Suzuri, “Nanometer-Thick SiN Films as Gas Barrier Coatings Densified by Vacuum UV Irradiation” Vol. 4, No. 10, pp. 10344-10353 (2021).
- [6] S. Hara, H. Yoshida, K. Arai, A. Uehigashi, K. Tate, T. Imamura, Y. Hosooka, “Development of Gas-Barrier-Property Evaluation System for High Sensitivity and Short Evaluation Time” *SID 2019 DIGEST*, vol. 50, No. 1, 1091-1093 (2019)